Asymmetric Operation of DAB Converter with Reduced Conduction Devices for Energy Storage Applications

Mahi Teja Talluri, V. Karthikeyan, *Member, IEEE*, Suganthi Ramasamy, *Member, IEEE*, Kashem M. Muttaqi, *Fellow, IEEE*, Gianluca Gatto, *Senior Member, IEEE*, and Amit Kumar, *Member, IEEE*

***Abstract*—This paper proposes an asymmetric operation of dual active bridge (DAB) bidirectional converter by reducing the conduction devices count which improves the operating efficiency. It also offers the advantages of elimination of circulating power flow (CPF), extension of soft switching region, reduction in current stress and smaller filter requirement. The paper describes the detailed operating waveforms and analysis of power transfer for the proposed asymmetric operation of the DAB converter. To analyze the accurate power dissipation in each power component the loss breakdown analysis is presented. The analytical results presented in this paper and proposed operation of the DAB converter has been verified through the experimental results.**

***Index Terms*—Asymmetric Operation, Circulating Power Flow (CPF), Current Stress, Dual Active Bridge (DAB).**

I. Introduction

THE Dual Active Bridge (DAB) converter offers seamless bidirectional power transfer at greater voltage conversion ratios while providing isolation. It offers several benefits including zero voltage switching (ZVS), zero current switching (ZCS), smooth power transfer, increased efficiency, and a reduced size. Yet, it is limited by circulating power flow (CPF), higher current stress, and a confined ZVS range. The circulation power flow defined as the power circulating in the high-frequency transformer, LV and HV bridges, based on the instantaneous difference in phase between the HV and LV bridges' output voltages. which flows due to negative portion of output/input current.

In an effort to address these limitations, numerous methods for modulation have been documented in the literature [1], [2], [3]. The single phase shift (SPS) is the simple modulation technique for regulating the transfer of power in a DAB converter. However, this causes increased current stress and a greater CPF across the entire power spectrum.

In [4], the dual phase shift (DPS) modulation scheme is proposed as a method to attain a broad power transfer range and adaptability in regulating transmission of power during low circulating power. [5] outlined the closed loop operation employed with DPS modulation to regulate power transmission for distribution grid applications.

A range of modulation techniques were proposed by researchers in [6], [7], [8], [9], [10], [11], [12] with the aim of improving the functionality of the DAB converter. Extended phase shift (EPS) modulation is suggested in [6] as a means to reduce the power consumed by the circulation at the input voltage end. However, at the output voltage end, it is vulnerable to circulation power. A hybrid modulation scheme has been proposed in [7], which minimizes the CPF and improves efficiency. In [8] triangle modulation is introduced as a means to achieve zero-current switching (ZCS) across the entire power spectrum. Nevertheless, its efficacy is dependent on the voltage conversion ratio exceeding unity, as highlighted in [9]. To address this limitation, an enhanced modulation technique was presented in [10]. The DAB converter often suffers from hard switching action which depends on the power and voltage conversion ratio. Many efforts have been made to extend the ZVS operation. The snubber/auxiliary circuits provide an optimal solution related to hard switching but it reflects additional losses and cost. RCD type snubber absorbs the voltage spikes during turn off but it leads to low efficiency. Different types of snubbers are proposed to avoid hard switching operation in [11], [12], [13], [14].

The efficiency of the DAB converter deteriorates due to presence of CPF. This paper is focused to eliminate the CPF by reducing the conduction switch count to improve the efficiency. The circulation power and current stress are increased when the voltage conversion ratio deviates from unity [15], [16], [17]. Several studies have explored methods to minimize current stress in DAB converters. A phase-shift modulation technique [18]

This work was supported in part by Project Network 4 Energy Sustainable Transition - NEST through the National Recovery and Resilience Plan (NRRP), in part by Mission 4, in part by Component 2, in part by Investment 1.3, through the Call for Tender No. 1561 dated October 11, 2022, under Grant PE0000021, in part by the Next-Generation EU Program, in part by the Italian Ministry of University and Research, and in part by Innovative Project Scheme CIEI/SIP/2023-24/01 through National Institute of Technology Calicut, Kerala, India. *(Corresponding authors: V. Karthikeyan; Amit Kumar.)*

Mahi Teja Talluri and V. Karthikeyan are with the Department of Electrical Engineering, National Institute of Technology, Kerala 673601, India (e-mail: mahitmt@gmail.com; karthi13546@gmail.com).

Suganthi Ramasamy, Gianluca Gatto, and Amit Kumar are with the Department of Electrical and Electronics Engineering, University of Cagliari, Via Marengo 2, 09123 Cagliari, Italy (e-mail: suganthi.ramasamy@unica.it; gatto@unica.it; amit.kumar@unica.it).

Kashem M. Muttaqi is with the School of Electrical, Computer and Telecommunications Engineering, University of Wollongong, New South Wales 2522, Australia (e-mail: kashem@uow.edu.au).

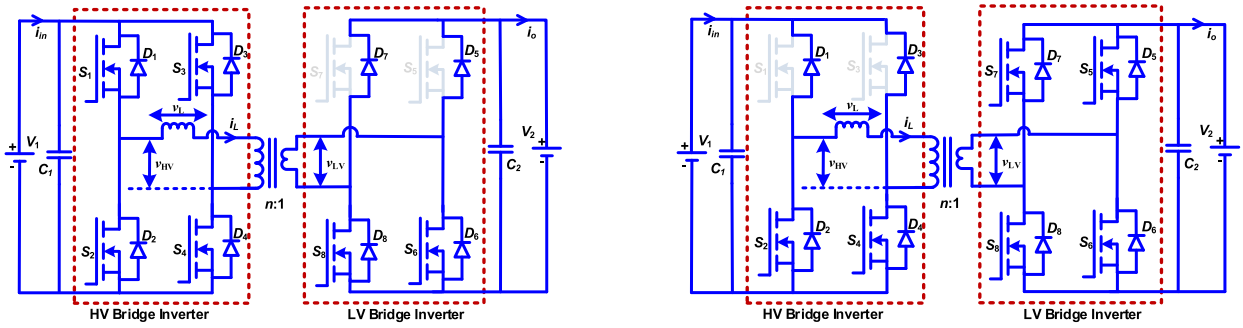

(a) (b)

Fig. 1 Proposed operation modes of DAB (a) Forward (b) Reverse.

and a hybrid modulation strategy [19] have been proposed to minimize current stress. A bidirectional DC–DC converter for EVs integrates PWM and Triple Phase Shift (TPS) modulation for efficiency and current stress reduction [20]. In [6], the current stress of DAB converter with EPS modulation has been analyzed which states that EPS has better flexibility in control with minimum current stress. In [16], zero circulating current (ZCC) modulation technique has been proposed to eliminate the CPF for entire operating range by introducing a limiting factor, and thereby it improves the efficiency. In comparison to DPS and SPS, DAB converters employs alternative modulation schemes, particularly those necessitating dynamic power transmission control, poses considerable challenges [5]. The Pulse Injection Modulation (PIM) method for Current-Fed Dual Active Bridge (CF-DAB) improves efficiency and reduces losses through optimized modulation timing [21]. In [22], a semi dual active bridge (S-DAB) converter is proposed to reduce the CPF and increase in efficiency. However, it is not suitable for bidirectional power transfer. In [23], a new DAB converter was proposed for medium power transfer application by reducing the number of devices. The active switches have been replaced with capacitor in one leg of the inverter. However, the converter is not suitable for high voltage conversion and large power transmission applications. The Hybrid-Type DAB (H-DAB) extends the voltage range using an auxiliary half-bridge and Extended Gain (EG) control, validated in a 500W prototype [24]. Recently in [25], a novel high-conversion ratio converter is proposed to obtain higher efficiency by reducing number of active devices. However, it has increased circuit complexity.

This paper proposes an asymmetric operation of DAB bidirectional converter in which two active switches are disabled to conduct in both forward and reverse mode of operation. Compared to conventional symmetric operation, and the novelty of this paper is to turn off a pair of switches during operation, resulting in an asymmetric mode for the entire operation, which increases power transfer capability, extends the soft switching range, and reduces the number of conduction devices,. and smaller filter requirement. thereby improving performance. For filter design, GaN-based DAB optimization [26] and phase-shift modelling [27] improve power density and performance. The soft switching boundaries of HV and LV bridges are presented in this paper. Analysis and experiments are performed to verify the proposed operation.

TABLE I
COMPARISON OF SEMICONDUCTOR DEVICE COUNT FOR CONVENTIONAL AND PROPOSED OPERATION OF DAB

Operation of DAB	Semiconductor device count				Total in each state
	Forward mode		Reverse mode		
	Switches	Diodes	Switches	Diodes	
Conventional	8	8	8	8	16
Proposed	6	8	6	8	14

II. PROPOSED ASYMMETRIC OPERATION OF DAB WITH SPS AND DPS MODULATION

The equivalent circuit of the proposed DAB converter in forward and reverse operating modes is shown in Fig. 1(a) and (b), respectively. When compared to a traditional DAB converter, the two active switches in both forward and reverse mode of operation are disabled and hence not in conduction state. Inductance L plays a crucial role in power transfer within a DAB converter. V_1 represents the input DC voltage, while V_2 represents the output DC voltage of the converter; n is turns ratio of high frequency transformer; C_1 and C_2 are the filter capacitance at input and output voltage end, respectively; i_{in} and i_{o} are the current flows at input and output respectively. v_{HV} and v_{LV} are the AC voltages across HV and LV bridges, respectively. The switches and diodes in Fig. 1 are denoted by S_{i} and D_{i} (where $i = 1, 2 \ldots .8$).

The count of semiconductor devices during conduction in each bridge of the DAB is compared in Table I for the proposed and conventional operation. It brings up that the proposed operation requires lesser number of conduction devices in both the mode of operation. Compared to conventional approach the loss of the DAB converter is reduced due to disabling of respective switches as shown in Fig. 1, hence it leads to increased efficiency. In forward mode, the switches S_5 and S_7 are in off state, which restricts the current to flow from source V_2. Similarly, in reverse mode the switches S_1 and S_3 are in off state, which restricts the current to flow from source V_1. As a result, the CPF gets eliminated in both the modes from the respective ends.

In the conventional symmetric operation, the switches S_5-S_7 in forward mode (S_1-S_3 in reverse mode) are in on state, but the current flows through freewheeling diodes D_5-D_7 (D_1-D_3 in reverse mode) and it leads to conduction losses in freewheeling

diodes. Once the inductor energy discharges through the freewheeling diodes the circulation current start flowing via switches S_5-S_7 from source V_2 due to their on-state condition. Hence, the switching and conduction losses due to circulation current occur in the respective switches. In the proposed asymmetric operation, during forward mode, the switches S_5-S_7 (S_1-S_3 in reverse mode) are in off state and the current flows through the freewheeling diodes D_5-D_7 (D_1-D_3 in reverse mode) similar to conventional operation. However, after inductor energy discharges through the freewheeling diodes there is no path for circulation current to flow due to off-state of switches S_5-S_7 in forward mode. Hence the additional switching and conduction losses are eliminated, thereby it improves the efficiency. Same is true in reverse mode. In addition, it eliminates the CPF and reduction in peak current stress of the switches. Compared to HV bridge inverter, the LV side inverter has to handle larger amount of current and with proposed operation the stress on switches get lowered and it results in better life service of switches. Among various modulation methods the global power transmission is the maximum with the SPS modulation and the power regulating capability is better with the DPS modulation. Hence, this paper details the proposed asymmetric operation of the DAB converter with SPS and DPS modulation and compares it with the conventional symmetric operation.

A) SPS Modulation

The HV and LV inverter bridge generates square voltage wave with a phase angle shift with respect to each other. Fig. 2(a) and (b) illustrate DAB converter's operating waveform. with SPS modulation for conventional symmetric and proposed operation, respectively and, d is the ratio of phase shift.

The voltage, input current and output current variations are shown in these figures. In SPS modulation with conventional operation, more circulation current flows at input and output voltage ends of the DAB. In proposed operation, once the inductor current reaches to zero, the LV bridge inverter gives zero voltage since the switches S_5 and S_7 remains off. It can be seen from Fig. 2(b) that the LV bridge inverter produces a three level voltage. Hence, the circulating current gets eliminated in i_o waveform as shown in Fig. 2(b), whereas in Fig. 2(a), the circulating current exits. As it is a well-known fact that the maximum power transmission can be achieved by keeping both HV and LV bridge output to be square wave. But in proposed operation of DAB in forward mode, the LV bridge produces three-level voltage; hence the global power transmission is reduced.

B) DPS Modulation

There are two modes of control with DPS modulation: i) $0 \leq d_1 \leq d_2 \leq 1$, and ii) $0 \leq d_2 < d_1 \leq 1$. Where, d_1 and d_2 are inner and outer phase shift ratios, respectively. Fig. 2(c) and (d) show the DAB converter's operating waveforms for the proposed operation. The switches S_5 and S_7 goes in off state in forward mode at t_5 and t_6 instant, for the condition $0 \leq d_1 \leq d_2 \leq 1$ and $0 \leq d_2 < d_1 \leq 1$, respectively. After this instant the circulation current at output voltage end becomes zero as shown in Fig. 2(c) and (d). It can be noted that in proposed asymmetric operation there is no negative current pulse in the output of the DAB as shown in Fig. 2(b)–(d), whereas in symmetric operation it exists as shown in Fig. 2(a). Absence of the circulation current at output voltage end reduces the rms AC current in the output capacitor; thereby DAB converter requires smaller filter capacitance.

III. Power Flow Analysis

It can be found that the current waveform remains same in every half cycle for both SPS and DPS modulation techniques. The proposed asymmetric operation of the DAB converter has an operating waveform similar to that of the symmetric operation, except during the time interval between t_1 to t_2 in SPS modulation. For DPS modulation, it is similar except during the time interval between t_2 to t_3 and t_1 to t_2, for the conditions, $0 \leq d_1 \leq d_2 \leq 1$ and $0 \leq d_2 < d_1 \leq 1$, respectively. The various peak inductor currents at different time instants can be determined from the following expressions.

$$\frac{di_L(t)}{dt} = \frac{(v_{HV}(t) - nv_{LV}(t))}{L} \tag{1}$$

When applying (1) in Fig. 2(b)–(d), at different instants, the expressions of the peak output current for the proposed operation with SPS modulation can be derived and listed in Table II. Where, $k = V_1/nV_2$ is the voltage conversion ratio and f is the switching frequency. The power transmission of the DAB can be found from the product of the average output current i_{o_avg} and output voltage V_2 and it can be written as follows.

$$p = i_{o\_avg} V_2 \tag{2}$$

i_{o_avg} can be determined by considering the area under the curve of i_o as shown in Fig. 2(b). The generalized power expression can be written for the SPS modulation as below.

$$I_{o\_avg} = \frac{1}{2f}\left[\left(\left(i_L(t_2) + i_{Lp}(t_3)\right)(1 - d_1 - x) + \left(i_L(t_2)d_1\right)\right] \tag{3}$$

By substituting the current expression listed in Table II at each time instant in (3), the average output current can be determined. Similarly, i_{o_avg} can be determined for DPS modulation in the proposed operation. Thereafter, by substituting the i_{o_avg} in (2), the power transmission expression can be found for SPS and DPS modulation in and listed in Table III. For convenient analysis, the unified power transmission for SPS and DPS control can be written in (4) and (5), respectively, as below.

$$p = \frac{P}{P_N}\left(\frac{4d}{9}(6 - 5d)\right) \quad for\ 0 \leq d \leq 1 \tag{4}$$

$$p = \frac{P}{P_N}$$
$$\begin{cases} \frac{4d_2}{9}(6 - 5d_2 - 5d_1) - \frac{d_1}{9}(6 - 7d_1) & 0 \leq d_1 \leq d_2 \leq 1 \\ 4d_2(1 - d_1 - \frac{1}{2}d_2) & 0 \leq d_2 < d_1 \leq 1 \end{cases} \tag{5}$$

Where P_N is the net power transmission in conventional operation and defined as

$$P_N = \frac{nV_1V_2}{8fL} \tag{6}$$

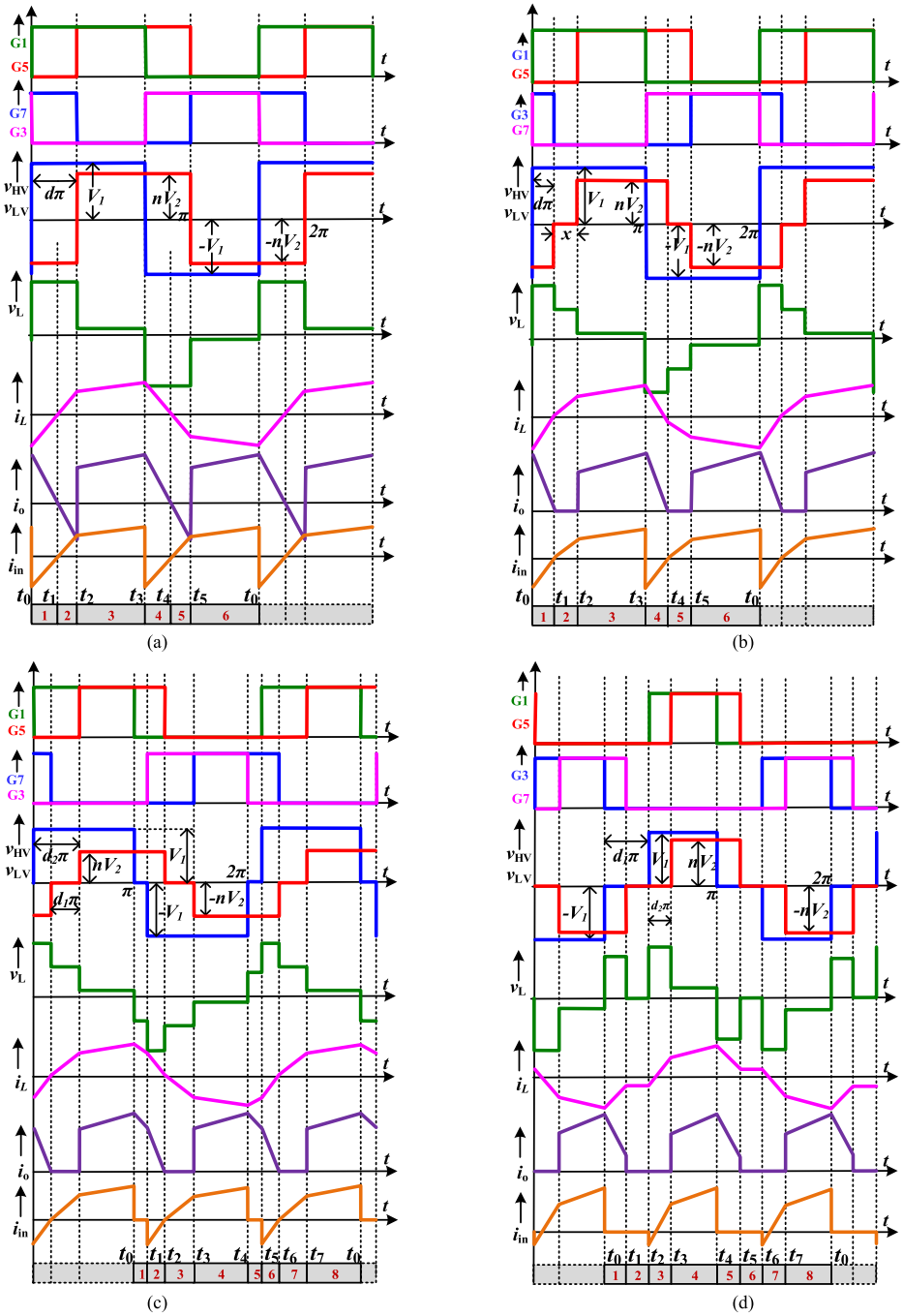

Fig. 2. Operating waveforms of DAB converter: (a) SPS modulation for symmetric, (b) SPS modulation for proposed asymmetric; and DPS modulation for proposed asymmetric (c) $0 \leq d_1 \leq d_2 \leq 1$, (d) $0 \leq d_2 < d_1 \leq 1$.

To achieve the power characterization, the maximum and minimum power has been obtained in [17] for the conventional operation of the DAB converter. In order to obtain the power characterization of the DAB converter for the proposed operation, the maximum power $P_{\max}$ and minimum power $P_{\min}$ has been derived below by considering the constraints $0 \leq d_1 \leq d_2 \leq 1$ and $0 \leq d_2 < d_1 \leq 1$ in (5).

For $0 \leq d_2 \leq 0.5$, the $P_{\max}$ and $P_{\min}$ can be written as

$$p_{\max} = \begin{cases} \frac{4d_2}{9}(6 - 5d_2) & d_1 = 0 \\ 2d_2(2 - 3d_2) & d_1 = d_2 \end{cases} \tag{7}$$

$$p_{\min} = \begin{cases} 2d_2(2 - 3d_2) & d_1 = d_2 \\ 2{d_2}^2 & d_1 = 1 - d_2 \end{cases} \tag{8}$$

TABLE II
VARIOUS PEAK CURRENTS OF INDUCTOR IN HALF SWITCHING CYCLE

Operating Mode	i_L	Value	i_L	Value
$0 \le d \le 1$ SPS	$i_o(t_2)$	$= \frac{nV_2}{2fL}\left[\frac{k}{2k+1}(2kd-k+1)\right]$	$i_o(t_3)$	$= \frac{nV_2}{2fL}\left[\frac{k+1}{2k+1}(k-1+d)\right]$
$0 \le d_2 \le d_1 \le 1$ (DPS)	$i_o(t_4)$	$= \frac{nV_2}{2fL}[(k-1)(1-d_1-d_2)]$	$i_o(t_5)$	$= \frac{nV_2}{2fL}[k(1-d_1-d_2)-(1-d_1)]$
$0 \le d_1 \le d_2 \le 1$ (DPS)	$i_o(t_3)$	$= \frac{nV_2}{2fL}\left[\frac{k}{2k+1}(2d_2+d_1)\right]$	$i_o(t_5)$	$= \frac{nV_2}{2fL}\left[\frac{k+1}{2k+1}(k(2d_2-d_1)-d_2\right]$
	$i_o(t_4)$	$= \frac{nV_2}{2fL}\left[\frac{k(k+d_2)+d_1(k+1)-1+d_2}{2k+1}\right]$		

TABLE III
POWER TRANSMISSION OF DAB FOR PA OPERATION USING SPS AND DPS CONTROL

Condition	P
$0 \le d \le 1$ (SPS)	$\frac{nV_1V_2}{2fL}\left[\frac{d}{9}(6-5d)\right]$
$0 \le d_1 \le d_2 \le 1$ (DPS)	$\frac{nV_1V_2}{2fL}\left[\frac{2d_2}{9}(6-5d_2-5d_1)+\frac{d_1}{9}(6-7d_1)\right]$
$0 \le d_2 \le d_1 \le 1$ (DPS)	$\frac{nV_1V_2}{2fL}\left[d_2(1-d_1-\frac{1}{2}d_2)\right]$

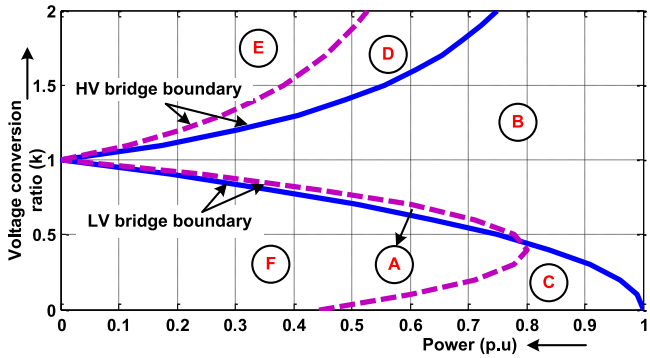

Fig. 4. Soft switching regions of DAB converter as a function of power (pu) and k.

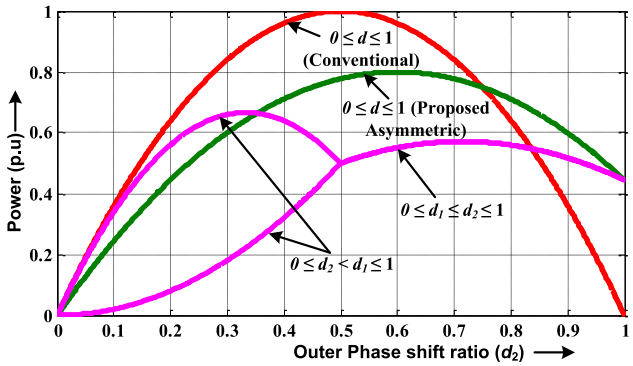

Fig. 3 Relation curves of the unified power transmission.

For $0.5 \le d_2 \le 1$, only $P_{\min}$ is applicable and can be written as

$$p_{\min} = \frac{2}{9}(10d_2 - 7{d_2}^2 - 1); \qquad d_1 = 1 - d_2 \tag{9}$$

Using (7) to (9), the power characterization for the proposed asymmetric operation of DAB with SPS and DPS control is shown in Fig. 3. Furthermore, using (6) the power transmission curve is compared with the conventional symmetric operation of the DAB with SPS control, which is also plotted in Fig. 3. It can be seen from Fig. 3, that the global power transmission in proposed operation is 0.8 times that of the conventional operation of the DAB. However, due to lesser number of device conduction and CPF elimination the efficiency will improve. When the power transfer requirement is more than 0.8, the asymmetric operation of the DAB needs to be switched over to the symmetric operation. In other words, the proposed asymmetric method is well-suited for light to medium load conditions, achieving efficient power transfer up to 80% of the rated power before requiring a shift to conventional SPS modulation. Similarly, for DPS modulation, power transfer is effective up to 65%, beyond which SPS modulation becomes necessary for optimal performance.

A) *Soft Switching Analysis*

In order to achieve ZVS, the DAB converter must operate with soft switching conditions of $i_o(t_2) > 0$ for the LV and $i_o(t_3) > 0$ for the HV bridge [12]. These inequalities in output currents satisfies for the following condition of phase shift ratio d obtained from first row of Table II and Fig. 2(b).

$$\text{For } i_L(t_2) > 0, \qquad d > \frac{k-1}{2k} \tag{10}$$

$$\text{For } i_L(t_3) > 0, \qquad d > 1 - k \tag{11}$$

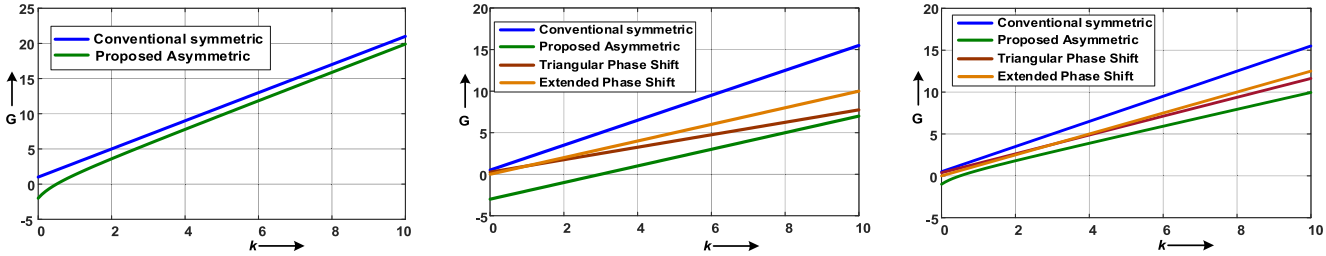

Fig. 5 Comparative unified current stress of DAB converter in (a) SPS modulation, and DPS modulation for (b) $0 \leq d_2 \leq d_1 \leq 1$, and (c) $0 \leq d_1 \leq d_2 \leq 1$.

Fig. 4 clearly depicts the regions of soft switching. The region B+C+D indicates soft switching, while the region A+E+F indicates hard switching for DAB using asymmetric SPS modulation.

Soft-switching region of A+B pertaining to CS operation

Soft switching region of B+C+D for PA operation

The hard switching region for PA operation is the area of A+E+F.

The region A+B denotes the soft switching area during symmetric operation. The area D represents the extended soft switching region with asymmetric operation. The circuit designers are usually interested in the voltage conversion ratio k and the unified power transfer characteristics of the DAB converter. It can be concluded that, the soft switching regions are extended in proposed asymmetric operation.

B) Comparative Analysis of Current Stress

For the purpose of comparison, the unified current stress G for the SPS symmetric [15] and proposed asymmetric operation is defined in (12) and (13), respectively.

$$G_{SPS-CS} = \frac{i_L(t_3)}{I_{avg}} = 2(2d - 1 + k) \tag{12}$$

$$G_{SPS-PA} = \frac{i_L(t_3)}{I_{avg}} = \frac{4(k+1)}{(2k+1)}(k - 1 + d) \tag{13}$$

Where

$$I_{avg} = \frac{P_0}{V_1} = \frac{nV_2}{8fL} \tag{14}$$

Fig. 5(a) shows the comparative current stress using (12) and (13), as a function of k. Similarly, the unified current stress of DAB converter with DPS modulation is defined in (15)–(18) below

i) $0 \leq d_2 \leq d_1 \leq 1$

$$G_{DPS-CS} = \frac{i_L(t_4)}{I_{avg}} = 2\left[k(1 - d_1) + (d_1 + 2d_2 - 1)\right] \tag{15}$$

$\leq d_1 \leq d_2 \leq 1$, are shown in Fig. 5(b) and (c), respectively

$$G_{DPS-PA} = \frac{i_L(t_4)}{I_{avg}} = \frac{4(k+1)}{(2k+1)}(k - 1 + d_2) \tag{16}$$

TABLE IV
EXPERIMENTAL SETUP PARAMETERS

Parameter	*Experiment*
V_1, V_2	30 V, 12 V
Converter Rated Power	180 W
Inductance (DAB converter)	5 µH
Switching Frequency	100 kHz
Nominal battery voltage	12 V
Transformer rating	100 kHz,1 kVA
Transformer Turn ratio	2:1

ii) $0 \leq d_1 \leq d_2 \leq 1$

$$G'_{DPS-CS} = \frac{i_L(t_4)}{I_{avg}} = 4\left[k(1 - d_1) + (d_1 + 2d_2 - 1)\right] \tag{17}$$

$$G'_{DPS-PA} = \frac{i_L(t_4)}{I_{avg}} = \frac{2(k+1)}{(2k+1)}(k - 1 + d_2) \tag{18}$$

Using (15)–(18), the comparative unified current stress of the DAB converter for the constraint of i) $0 \leq d_2 \leq d_1 \leq 1$ and ii) $0 \leq d_1 \leq d_2 \leq 1$, are shown in Fig. 5(b) and (c), respectively.

As observed from Fig. 5, the current stress increases proportionally with the voltage conversion ratio k across the entire operating region. The proposed asymmetric operation effectively reduces the current stress in the DAB converter compared to conventional symmetric operation. Furthermore, the current stress performance of the proposed asymmetric modulation is compared with other popular reported techniques, including SPS, TPS, and EPS in Fig. 5(b) and (c). The results demonstrate that the proposed approach achieves lower current stress than the conventional symmetric method while maintaining competitive performance with advanced modulation techniques. The comparative analysis is performed considering the parameters listed in Table IV. The peak current stress of the output has been measured in the symmetric and proposed asymmetric operation, which is shown in Fig. 6. The current stress of symmetric operation is consistently higher than that of asymmetric operation at the same power transmission.

IV EXPERIMENTAL RESULTS

In order to validate the analysis mentioned above, an experimental setup developed and executed employing a controller FPGA Spartan 3AN processor. The experimental waveforms

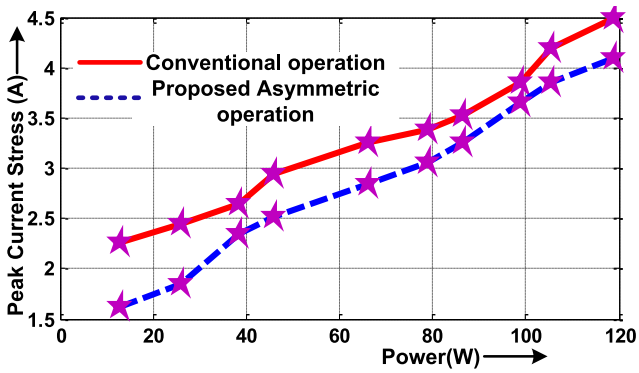

Fig. 6 Comparison of current stress for conventional and proposed asymmetric operation of DAB converter.

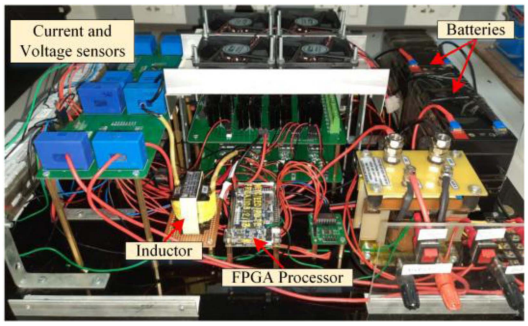

Fig. 7 Laboratory experimental set up.

of v_{HV}, v_{LV}, i_{o} and i_{in}, have been obtained for the following parameters listed in Table IV.

At a frequency of 100 kHz, the tests have been conducted for both square and PWM waveforms in both H bridges. In normal operation, the voltage conversion ratio k is thought to be 1.25. The HV and LV bridges are considered identical. To handle higher current ratings, PCB tracks reinforced with copper strips and IRF250N MOSFET devices are used in the bridges. While the intrinsic body diode of the MOSFET is sufficient for low and medium power applications, high-power applications require the integration of dedicated ultra-fast recovery diodes. The laboratory experimental set up is shown in Fig. 7. In order to implement the proposed asymmetric operation additional control logic of disabling the respective switching pattern based on power transfer direction has been incorporated. The experimental outcomes of the proposed asymmetric operation of DAB with SPS and DPS modulation are illustrated in Figs. 8 to 12 and verified. The results for v_{HV}, v_{LV}, i_{o} and i_{in} with SPS modulation in symmetric and proposed asymmetric operations are shown in Fig. 8(a) and (b), respectively.

As seen from Fig. 8(b), it validates zero circulation current at output voltage end with asymmetric operation, whereas in symmetric operation it exists as shown in Fig. 8(a).

Similarly, in reverse mode of operation the experimental results have been obtained and presented in Fig. 9(a) and (b) for symmetric and proposed asymmetric operations, respectively. Aforementioned theory presented in section II, the LV and HV

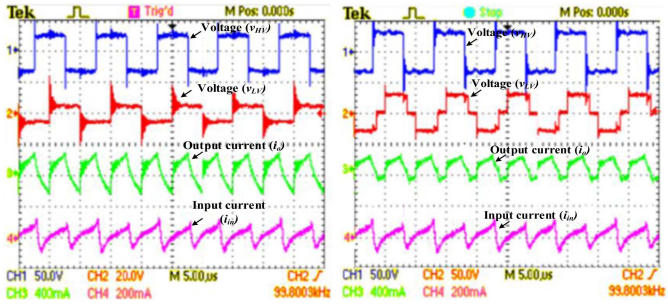

(a) (b)

Fig. 8 Experimental results showing v_{HV} (CH1), v_{LV} (CH2), i_{o} (CH3) and i_{in} (CH4) with SPS modulation in forward mode for (a) symmetric, (b) proposed asymmetric operation.

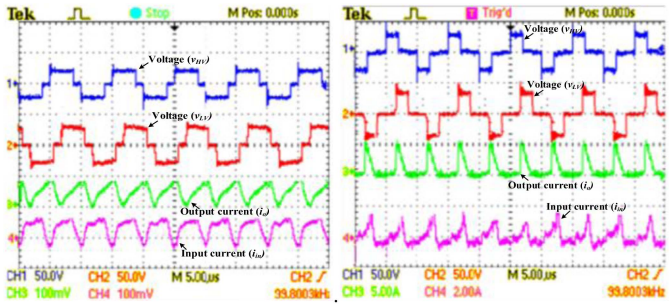

(a) (b)

Fig. 9 Experimental results showing v_{HV} (CH1), v_{LV} (CH2), i_{o} (CH3) and i_{in} (CH4) under DPS modulation in forward mode for (a) $0 \leq d_1 \leq d_2 \leq 1$, (b) $0 \leq d_2 < d_1 \leq 1$.

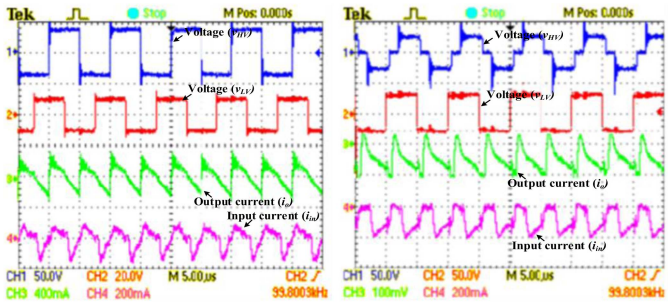

(a) (b)

Fig. 10 Experimental results showing v_{HV} (CH1), v_{LV} (CH2), i_{o} (CH3) and i_{in} (CH4) with SPS modulation in reverse mode for mode for (a) symmetric, (b) proposed asymmetric operation.

bridges produce a three-level voltage in forward and reverse mode, respectively in asymmetric operation, which can be validated by the experimental results of Figs. 8 and 9. To confirm the proposed asymmetric operation in forward mode with DPS modulation, the experimental results are displayed in Fig. 10(a) and (b), for the conditions i) $0 \leq d_2 \leq d_1 \leq 1$ and ii) $0 \leq d_1 \leq d_2 \leq 1$, respectively.

Similarly, Fig. 11(a) and (b) shows the experimental results with DPS modulation in reverse mode of asymmetric operation. As discussed earlier, the peak current stress of DAB increases

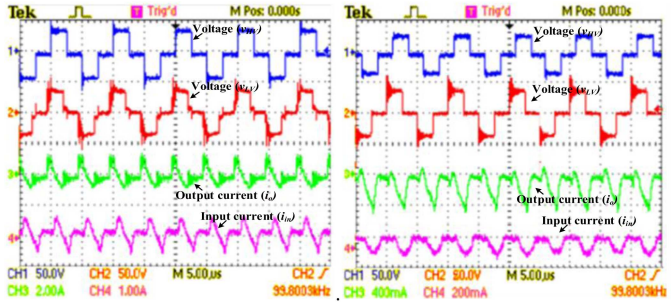

(a) (b)

Fig. 11 Experimental results showing v_{HV} (CH1), v_{LV} (CH2), i_{o} (CH3) and i_{in} (CH4) with DPS modulation in reverse mode for (a) $0 \leq d_1 \leq d_2 \leq 1$, (b) $0 \leq d_2 < d_1 \leq 1$.

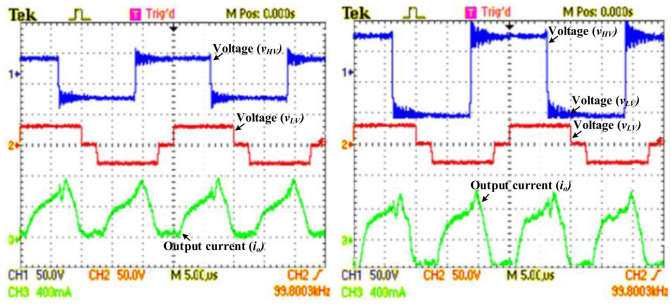

(a) (b)

Fig. 12 Experimental results showing v_{HV} (CH1), v_{LV} (CH2), and i_{o} (CH3) under DPS control for (i) $0 \leq d_1 \leq d_2 \leq 1$, (ii) $0 \leq d_2 < d_1 \leq 1$.

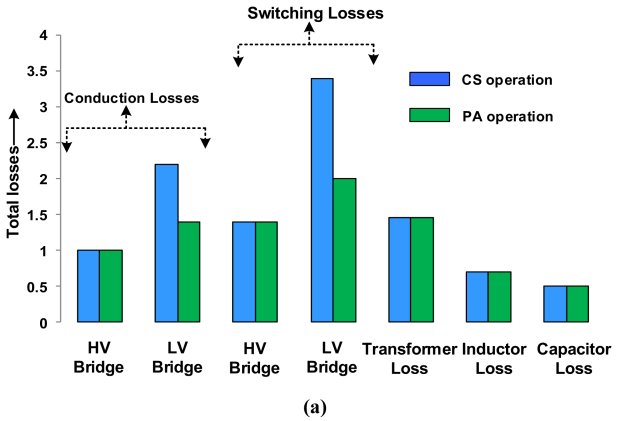

(a)

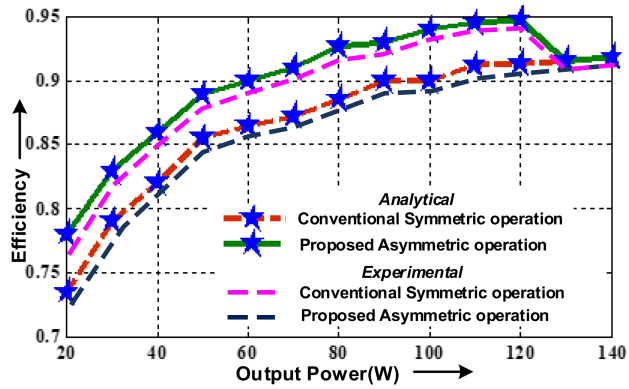

(b)

Fig. 13 (a) Loss breakdown of DAB converter with proposed asymmetric operation, (b) comparative analytical and experimental efficiency graph for symmetric and proposed asymmetric operation of DAB with variation of power transmission.

proportional to k. To confirm this experimental result is captured for $k = 1.75$ and 2.5 in forward mode of operation with SPS in Fig. 12(a) and (b), respectively. Fig. 12(a) and (b), shows the changes in i_{o} follows with respect to V_{HV} and V_{LV}. It clears that the peak current stress increases in proportion to k.

A. Loss Estimation

The efficiency of the DAB converter in the proposed asymmetric operation can be estimated using cumulative losses in the converter [28], [29]. A loss breakdown in the DAB converter has been considered. The total power losses PL_{total} of the DAB converter can be evaluated as below,

$$PL_{total} = P_{sw-HV} + P_{sw-LV} + P_{cond-HV} + P_{cond-LV} + P_{tr} + P_L + P_C \quad (19)$$

where $P_{\mathrm{sw\text{-}HV}}$ and $P_{\mathrm{sw\text{-}LV}}$ are switching losses of the HV and LV bridge, respectively; $P_{\mathrm{cond\text{-}HV}}$ and $P_{\mathrm{cond\text{-}LV}}$ are the conduction losses of the HV and LV bridge, respectively; P_{tr} is the transformer loss; P_{L} and P_{C} are the inductor and capacitor losses, respectively.

The loss breakdown of the DAB converter is shown in Fig. 13(a). From the estimated loss, it is observed that the switching loss of 4.9 W contributes more than other losses in the DAB converter. Finally, the comparative efficiency is measured and plotted in Fig. 13(b), with respect to power transfer for conventional symmetric and proposed asymmetric operation of the DAB. It can be seen from the figure that the efficiency with the proposed asymmetric operation increases by 4%. The efficiency graph converges to conventional symmetric operation beyond 80% of power transmission as explained earlier.

V. Conclusion

This paper proposes an asymmetric operation of DAB converter to enhance the efficiency by reducing the conduction devices count and elimination of CPF. The detailed operating waveform for the proposed asymmetric operation of the DAB converter and the analysis of power transmission with SPS and DPS modulation has been discussed. The proposed asymmetric operation offers the important advantages of circulation power flow (CPF) elimination at output voltage end, reduction in current stress, extension of soft switching region and smaller filter requirement. The range of soft switching for LV and HV bridge inverters are extended in the asymmetric operation compared to symmetric operation. The experimental results validate the proposed asymmetric operation of the DAB converter. The power dissipation has been obtained through the loss breakdown analysis to measure the efficiency. The proposed asymmetric operation expands the efficiency upto 4%. However, it has the limitation of power transmission up to 0.8 times of symmetric operation. Hence the efficiency improvement can be achieved

up till 0.8 times of maximum power transmission and thereafter the efficiency is equal to conventional symmetric operation of the DAB converter.

REFERENCES

[1] R. R. Khorasani et al., "An interleaved soft switched high step-up boost converter with high power density for renewable energy applications," *IEEE Trans. Power Electron.*, vol. 37, no. 11, pp. 13782–13798, Nov. 2022.

[2] D. Yadeo and P. Chaturvedi, "Performance characterization of T-type multilevel dual active bridge DC-DC converter," *IEEE Trans. Ind. Appl.*, vol. 59, no. 2, pp. 1877–1886, Mar./Apr. 2023.

[3] G. Oggier, G. O. Garc´ıa, and A. R. Oliva, "Modulation strategy to operate the dual active bridge dc-dc converter under soft switching in the whole operating range," *IEEE Trans. Power Electron.*, vol. 26, no. 4, pp. 1228–1236, Apr. 2011.

[4] P. Liu, C. Chen, S. Duan, and W. Zh, "Dual phase-shifted modulation strategy for the three-level dual active bridge DC–DC converter," *IEEE Trans. Ind. Electron.*, vol. 64, no. 10, pp. 7819–7830, Oct. 2017.

[5] V. Karthikeyan and R. Gupta, "Closed-loop control of isolated dual active bridge converter using dual phase shift modulation," in *IECON 2015 - 41st Annu. Conf. IEEE Ind. Electron. Soc.*, Yokohama, Japan, 2015, pp. 2800–2805.

[6] Q. Bu, H. Wen, H. Shi, and Y. Zhu, "A comparative review of high-frequency transient DC bias current mitigation strategies in dual-active-bridge DC–DC converters under phase-shift modulations," *IEEE Trans. Ind. Appl.*, vol. 58, no. 2, pp. 2166–2182, Mar./Apr. 2021.

[7] D. Mou et al., "Hybrid duty modulation for dual active bridge converter to minimize RMS current and extend soft-switching range using the frequency domain analysis," *IEEE Trans. Power Electron.*, vol. 36, no. 4, pp. 4738–4751, Apr. 2021.

[8] Q. Zhou et al., "A step-down resonant modular multilevel DC/DC converter with extendable ZVS range based on asymmetric triangular current," *IEEE Trans. Ind. Electron.*, vol. 69, no. 11, pp. 11088–11099, Apr. 2022.

[9] G. Xu, D. Sha, Y. Xu, and X. Liao, "Dual-transformer-based DAB converter with wide ZVS range for wide voltage conversion gain application," *IEEE Trans. Ind. Electron.*, vol. 65, no. 4, pp. 3306–3316, Apr. 2018.

[10] D. Das and K. Basu, "Optimal design of a dual-active-bridge DC–DC converter," *IEEE Trans. Ind. Electron.*, vol. 68, no. 12, pp. 12034–12045, Dec. 2021.

[11] I. Alhurayyis, A. Elkhateb, and J. Morrow, "Isolated and nonisolated DC-to-DC converters for medium-voltage DC networks: A review," *IEEE J. Emerg. Sel. Topics Power Electron.*, vol. 9, no. 6, pp. 7486–7500, Dec. 2021.

[12] Z. Guo, Y. Zhu, and D. Sha, "Zero-voltage-switching asymmetrical PWM full-bridge DC–DC converter with reduced circulating current," *IEEE Trans. Ind. Electron.*, vol. 68, no. 5, pp. 3840–3853, May 2021.

[13] X. Zhou et al., "A high-efficiency high-power-density on-board low-voltage DC–DC converter for electric vehicles application," *IEEE Trans. Power Electron.*, vol. 36, no. 11, pp. 12781–12794, Nov. 2021.

[14] P. Xuewei, A. K. Rathore, and U. R. Prasanna, "Novel soft-switching snubberless naturally clamped current-fed full-bridge front-end-converter-based bidirectional inverter for renewables, microgrid, and UPS applications," *IEEE Trans. Ind. Appl.*, vol. 50, no. 6, pp. 4132–4141, Nov./Dec. 2014.

[15] B. Zhao, Q. Song, W. Liu, and W. Sun, "Current-stress-optimized switching strategy of isolated bidirectional DC–DC converter with dual-phase-shift control," *IEEE Trans. Ind. Electron.*, vol. 60. no. 10, pp. 4458–4467, Oct. 2013.

[16] V. Karthikeyan and R. Gupta, "Zero circulating current modulation for isolated bidirectional dual-active-bridge DC–DC converter," *IET Power Electron.*, vol. 9, no. 7, pp. 1553–1561, 2016.

[17] B. Zhao, Q. Song, and W. Liu, "Power characterization of isolated bidirectional dual-active-bridge DC–DC converter with dual-phase-shift control," *IEEE Trans. Power Electron.*, vol. 27, no. 9, pp. 4172–4176, Sep. 2012.

[18] A. Rashwan, A. I. M. Ali, and T. Senjyu, "Current stress minimization for isolated dual active bridge DC–DC converter," *Sci. Reports*, vol. 12, no. 1, 2022, Art. no. 16980.

[19] J. Gong et al., "A current-stress-optimized control strategy for DAB converter using hybrid modulation," in *Proc. IECON 2020 46th Annu. Conf. IEEE Ind. Electron. Soc.*, Singapore, 2020, pp. 1148–1153.

[20] Y. Wang, Y. Li, Y. Guan, and D. Xu, "Topology and control optimization of bidirectional DC/DC converter for electric vehicles," *IEEE J. Emerg. Sel. Topics Power Electron.*, vol. 12, no. 1, pp. 257–268, Feb. 2024.

[21] C. Liu, X. Zou, S. Zhou, H. Peng, and Y. Kang, "Pulse injection modulation method for current-fed dual active bridge converter with full load range ZVS under wide input-voltage range," *IEEE Trans. Power Electron.*, vol. 40, no. 2, pp. 2668–2673, Feb. 2025.

[22] S. Kulasekaran and R. Ayyanar, "Analysis, design, and experimental results of the semi dual-active-bridge converter," *IEEE Trans. Power Electron.*, vol. 29, no. 10, pp. 5136–5147, Oct. 2014.

[23] B. Krishna and V. Karthikeyan, "A novel bi-directional high-gain DC-DC converter with optimum number of components," *Int. J. Circuit Theory Appl.*, vol. 51, no. 1, pp. 283–301, 2023.

[24] C. Liu, S. Liu, Y. Chen, X. Zou, and Y. Kang, "Hybrid-type dual active bridge DC–DC converter for ultrawide input-voltage range," *IEEE Trans. Power Electron.*, vol. 38, no. 9, pp. 10651–10668, Sep. 2023.

[25] T. J. Liang and J. H. Lee, "Novel high-conversion-ratio high-efficiency isolated bidirectional DC–DC converter," *IEEE Trans. Ind. Electron.*, vol. 62, no. 7, pp. 4492–4503, Jul. 2015.

[26] S. I. Hasan et al., "Design, optimization, and validation of GaN-based DAB converter for active cell balancing in BTMS applications," in *Proc. 2023 IEEE Energy Convers. Congr. Expo.*, Nashville, TN, USA, 2023, pp. 434–441.

[27] G. de Freitas Lima, Y. Lembeye, F. Ndagijimana, and J.-C. Crebier, "Modeling of a DAB under phase-shift modulation for design and DM input current filter optimization," in *Proc. 2020 22nd Eur. Conf. Power Electron. Appl.*, Lyon, France, 2020, pp. P.1–P.10.

[28] F. Krismer and J. W. Kolar, "Accurate power loss model derivation of a high-current dual active bridge converter for an automotive application," *IEEE Trans. Ind. Electron.*, vol. 57, no. 3, pp. 881–891, Mar. 2010.

[29] B. Krishna and V. Karthikeyan, "Ultra-voltage gain step-up DC-DC converter for renewable energy micro-source applications," *IEEE Trans. Energy Convers.*, vol. 37, no. 2, pp. 947–957, Jun. 2022.